Dalton Transactions

Accepted Manuscript

ROYAL SOCIETY OF CHEMISTRY

www.rsc.org/dalton

Dalton Transactions

RSCPublishing

ARTICLE

Tunable blue-green emission and energy transfer properties in β-$Ca_3(PO_4)_2$:Eu^{2+}, Tb^{3+} phosphors with high quantum efficiencies for UV-LEDs

Kai Li,[a,b] Yang Zhang,[a,b] Xuejiao Li,[a] Mengmeng Shang,[a] Hongzhou Lian*,[a] and Jun Lin*,[a]

Cite this: DOI: 10.1039/x0xx00000x

Received,
Accepted

DOI: 10.1039/x0xx00000x

www.rsc.org/

A series of Eu^{2+} and Tb^{3+} singly doped and co-doped β-$Ca_3(PO_4)_2$ phosphors have been synthesized via the high-temperature solid-state reaction method. The thermogravimetric (TG) analysis, fourier transform infrared (FT-IR) spectra, X-ray diffraction (XRD) patterns and Rietveld refinements, photoluminescence (PL) spectra including temperature-dependent PL and quantum efficiency, and fluorescence decay lifetimes have been used to character the as-prepared samples. Under UV excitation, the β-$Ca_3(PO_4)_2$:Eu^{2+} presents a broad emission band centered at 415 nm, which can be decomposed into five symmetrical bands peaking at 390, 408, 421, 435 and 511 nm based on substitutions of five kinds of Ca^{2+} sites by Eu^{2+} ions. The β-$Ca_3(PO_4)_2$:Tb^{3+} shows its characteristic emission lines under Tb^{3+} 4f-5d transition excitation around 223 nm. In β-$Ca_3(PO_4)_2$:Eu^{2+}, Tb^{3+} phosphors, the similar excitation spectra monitored at 415 and 547 nm have been observed, which illustrates the possibility of energy transfer from Eu^{2+} to Tb^{3+} ions. The variations of emission spectra and decay lifetimes further demonstrate the existence of energy transfer from Eu^{2+} to Tb^{3+} ions under UV excitation. The energy transfer mechanism has been certified to be dipole-quadrupole, which can be validated via the agreement of critical distances obtained from the concentration quenching (12.11 Å) and spectrum overlap methods (9.9-13.2 Å). The best quantum efficiency can reach 90% for β-$Ca_3(PO_4)_2$:$0.01Eu^{2+}$, $0.15Tb^{3+}$ sample under 280 nm excitation. These results show the developed phosphors may possess the potential application in UV-pumped white lighting-emitting diodes.

1. Introduction

Recently, rare earth ions doped inorganic materials have been extensively investigated because of their applications in many aspects such as optical, magnetic, catalytic devices.[1-3] In lighting field, white light-emitting diodes (wLEDs), the next generation of solid-state lighting source, are considered to replace the conventional incandescent and implemented fluorescent lamps attributed to their superior merits such as compactness, energy saving characteristic, high efficiency, long operation time besides no contamination to environment.[4-6] Currently, the major fabrication technique of wLEDs depends on the combination of a blue InGaN chip with the yellow-emitting phosphor $Y_3Al_5O_{12}$:Ce (YAG).[7] However, the deficiency of red component arouses the poor color rendering indices (CRI) and a high correlated color temperature (CCT), which limits the constant use in future. Therefore, the development of the technique by combining a UV LED chip with tricolor (blue, green, red) phosphors has been proceeding since it can produce high quality white emission LED. In this case, recent investigations have been focused on searching conversion luminescent phosphors with appropriate emission colors, high efficiency and high chemical stability.

Tb^{3+}, a well-known activator, can emit green color owing to its general $^5D_4$-$^7F_5$ transition corresponding to the emission peak around 545 nm.[8-10] It is a pity that the absorption peaks of Tb^{3+} in the UV region above 260 nm is rather weak and the widths of them are narrow because these transitions belong to the severe 4f-4f forbidden ones. However, the energy transfer from the host or sensitizer to activator in many inorganic hosts such as molybdates, phosphates, silicates, borates, and aluminates[11-20] have been demonstrated to be effective, which induce the intense emissions of Tb^{3+} under UV excitation. As a good activator, Eu^{2+} has been applied in many hosts and can emit different colors, such as blue for $BaCa_2MgSi_2O_8$:Eu^{2+}, green for $Ca_3Si_2O_4N_2$:Eu^{2+}, yellow for $Sr_8MgLu(PO_4)_7$:Eu^{2+},

[a]State Key Laboratory of Rare Earth Resource Utilization, Changchun Institute of Applied Chemistry, Chinese Academy of Sciences, Changchun 130022 (P. R., China.). Email: jlin@ciac.ac.cn;
Fax: +86-431-85698041; Tel: +86-431-85262031
[b]University of Chinese Academy of Sciences, Beijing 100049 (P. R., China.)

and red for $Ca_{15}Si_{20}O_{10}N_{30}:Eu^{2+}$.[21-24] Beside, it can be an appropriate sensitizer for Tb^{3+} in some hosts.[25-26] Therefore, the couple of Eu^{2+}/Tb^{3+} can act as the green component due to the absorption in UV area of Eu^{2+} and efficient energy transfer from Eu^{2+} to Tb^{3+} ions.

The phosphors involving similar β-$Ca_3(PO_4)_2$ whitlockite-type structure have been investigated such as $Ca_9MgNa(PO_4)_7:Ce^{3+},Tb^{3+},Mn^{2+}$,[14] $Ca_9Ln(PO_4)_7:Eu^{2+},Mn^{2+}$ (Ln = La, Gd, Lu),[27-29] $Ca_9Lu(PO_4)_7:Ce^{3+},Mn^{2+}$,[30] $(Ca,Mg,Sr)_9Y(PO_4)_7:Eu^{2+},Mn^{2+}$,[31] $Ca_{10}Li(PO_4)_7:Eu^{3+}$,[32] $Ca_9ZnLi(PO_4)_7:Eu^{3+}$,[33] $Ca_8MgR(PO_4)_7$ (R = La, Gd, Y):Eu^{3+},[34] $Ca_9LiGd_{2/3}(PO_4)_7:Eu^{3+}$,[35] $Ca_9R(PO_4)_7$ (R =Al, Lu):Eu^{3+},[36] and so on.[37] The results indicate that $Eu^{3+}/Eu^{2+}/Ce^{3+}$ are the good activators, and Eu^{2+}/Ce^{3+} can be served as effective activators to sensitize Mn^{2+} ions in whitlockite-type structure compounds. However, there are rare reports concerned the energy transfer phenomenon from Eu^{2+} to Tb^{3+} ions in such hosts. Herein, we have synthesized the Eu^{2+}, Tb^{3+} co-doped β-$Ca_3(PO_4)_2$ phosphors and investigated their photoluminescence (PL) properties as well as the sensitization behavior from Eu^{2+} to Tb^{3+} ions in β-$Ca_3(PO_4)_2$ host, which present intense tunable blue-green emission and high quantum efficiencies in β-$Ca_3(PO_4)_2:Eu^{2+}$, Tb^{3+} upon UV excitation, showing their potential application for UV-pumped wLEDs.

2. Experiment section

2.1 Materials and preparation

The objective β-$Ca_3(PO_4)_2:Eu^{2+}$, Tb^{3+} (abbreviated as β-CPO:Eu^{2+}, Tb^{3+}) phosphors were prepared via the high-temperature solid-state reaction route. The Eu^{2+} and Tb^{3+} ions were considered to substitute Ca^{2+} ions. Raw materials including $CaCO_3$ (A.R.), $NH_4H_2PO_4$ (A.R.), Eu_2O_3 (99.99%), Tb_4O_7 (99.99%) without any purification were mixed and ground thoroughly in an agate mortar for 15 min with an appropriate amount of ethanol followed by drying at 65 °C for 20 min in a bake oven. After being reground for 2min, the powder mixtures were transferred to the alumina crucibles and calcined in the tube furnace at 1150 °C for 6 h in a reducing atmosphere of H_2 (10%) and N_2 (90%) to generate the final samples. Then, the samples in room temperature were ground for about 1 min to be used for subsequent measurements.

2.2 Characterization

The X-ray diffraction (XRD) patterns were performed on a D8 Focus diffractometer at a scanning rate of 10°min^{-1} in the 2θ range from 10° to 110° with graphite-monochromatized Cu Kα radiation (λ = 0.15405 nm). Infrared spectra were collected on a VERTEX 70 Fourier transform infrared (FT-IR) spectrometer (Bruker).The PL measurements were conducted with a Hitachi F-7000 spectrophotometer equipped with a 150 W xenon lamp as the excitation source. The luminescence decay lifetimes were attained from a Lecroy Wave Runner 6100 Digital Osilloscope (1 GHz) using a tunable laser (pulse width = 4 ns, gate = 50 ns) as the excitation (Contimuum Sunlite OPO) source. PL quantum yields (QYs) of phosphors were obtained directly by the absolute PL quantum yield measurement system (C9920−02, Hamamatsu Photonics K. K., Japan). All the above measurements were carried out at room temperature (RT). Besides, the PL emission spectra of the phosphor depending on temperature were measured on a Horiba Jobin-Yvon Fluorolog-3 FL3-211pectrometer equipped with a 450 W xenon lamp as the excitation source. Moreover, Thermogravimetry analysis (TGA) was proceeded on a Netzsch STA 409 thermoanalyzer with a heating rate of 5 °C/min in air atmosphere from room temperature to 1200 °C.

3. Results and discussions

3.1 TGA and FT-IR analyses

As depicted in Fig. 1, the DSC-TG curves of β-CPO:0.01Eu^{2+}, 0.20Tb^{3+} were investigated to analyze the pyrolysis behavior and crystallization process, which indicates that the weight loss of precursor take place from room temperature until at about 850 °C in the TG curve. It is apparent that there are four rough stages in the whole operated temperature range according to TG-DSC curves. The first stage can be assigned to the slight loss of about 2% from 25 to approximate 200 °C in the TG curve, which mostly corresponds to the volatilization of the absorbed water. The second stage can be found from 200 to about 650 °C with the sharp loss of about 22%, which is attributed to the decomposition of phosphate in the starting materials due to its low decomposition temperature. After that, the decomposition of $CaCO_3$ arouses the decrease of mass of materials, which corresponds to the exothermic peak around 808 °C in the DSC curve. Then, the mass continue to decrease

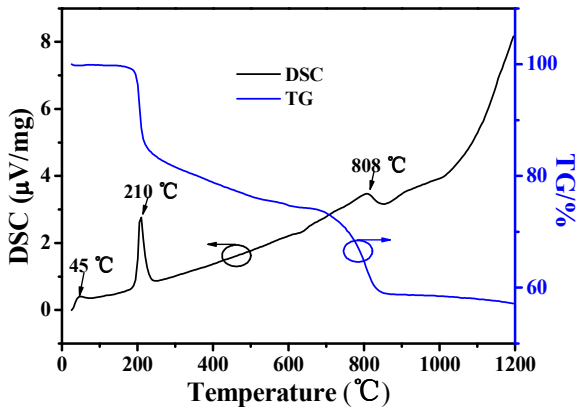

Fig. 1 The DSC-TG curves of raw materials from room temperature to up to 1200℃ with a heating rate of 5 ℃/min in air.

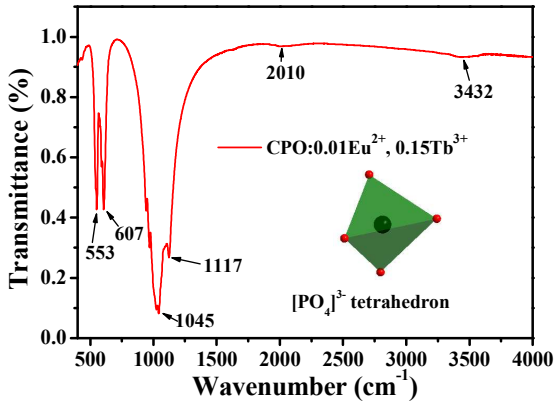

Fig. 2 FT-IR spectrum of as-prepared representative β-CPO:0.01Eu^{2+}, 0.15Tb^{3+} sample.

minor extended to 1200 °C due to the decomposition of a small quantity of $CaCO_3$ which are un-decomposed. Simultaneously, the β-CPO phase starts to be formed.

To recognize the existence of orthophosphate in our synthesized samples, the FT-IR spectra of representative β-CPO:0.01Eu^{2+}, 0.15Tb^{3+} was measured and plotted in Fig. 2. In general, the IR absorption band of $(PO_4)^{3-}$ locates at 650-540 cm^{-1} and 1120-940 cm^{-1},[38] which contains four absorption peaks at 553 and 607, and 1045 and 1117 cm^{-1} here, respectively, originating from the symmetric stretching mode of $(PO_4)^{3-}$ units. Another two peaks at 2010 and 3432 cm^{-1} can be assigned to OH^- vibrations which derive from the covered water on the surface of phosphors under air condition. The result indicates that orthophosphate exists in this compound, which can be deduced in these series samples.

3.2 Phase identification and purity

In order to determine the phase composition and their purity of as-prepared powder samples, they were detected by XRD. Fig. 3 shows the representative XRD patterns of β-CPO:0.01Eu^{2+}, β-CPO:0.20Tb^{3+} and β-CPO:0.01Eu^{2+}, 0.20Tb^{3+} as well as the standard pattern of β-CPO. It is obvious that all the diffraction peaks are indexed to the pure phase of β-$Ca_3(PO_4)_2$ (JCPDS 09-0169) with almost no impurity, indicating that all the as-prepared samples are crystallized in the single phase. Fig. 4 shows the crystal structure of β-CPO and the different coordination environment for Ca atoms. β-$Ca_3(PO_4)_2$ has a crystalline rhombohedral system with space group *R3c* (167), and the lattice parameters as $a = b = 10.4352(2)$ Å, $c = 37.4029(5)$ Å, $\alpha = \beta = 90°$, $\gamma = 120°$, $V = 3520.91$ Å^3, and $Z = 21$.[39] It is clearly seen there are five kinds of Ca lattice positions in the structure, which are coordinated by seven oxygen atoms around for Ca1, eight for Ca2, eight for Ca3, three for Ca4, and six for Ca5, respectively. It is worth noting that the Ca4 is threefold coordinated, suggesting weak bonding and the formation of deficiency,[39] and it has a planar shape as shown in Fig. 4. The incorporations of Eu^{2+} and Tb^{3+} ions are expected to substitute Ca^{2+} lattice positions based on their ionic radii [r(Eu^{2+}) = 1.17 Å, r(Tb^{3+}) = 0.92 Å and r(Ca^{2+}) = 1.00 Å for coordination number (CN) = 6, r(Eu^{2+}) = 1.20 Å, r(Tb^{3+}) = 1.02 Å and r(Ca^{2+}) = 1.07 Å for CN = 7, r(Eu^{2+}) = 1.25 Å, r(Tb^{3+}) = 1.04 Å and r(Ca^{2+}) = 1.12 Å for CN = 8], respectively, while the r(P^{5+}) = 0.17 Å is too small to be occupied by Eu^{2+}/Tb^{3+}. The Rietveld refinement of XRD patterns of representative β-

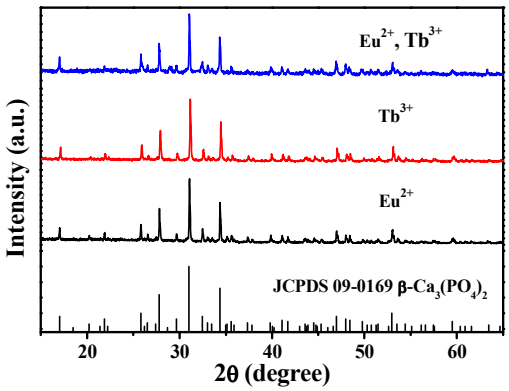

Fig. 3 Representative XRD patterns of β-CPO:0.01Eu^{2+}, β-CPO:0.20Tb^{3+} and β-CPO:0.01Eu^{2+}, 0.20Tb^{3+} as well as the standard reference of β-$Ca_3(PO_4)_2$ (JCPDS Card No. 09-0169).

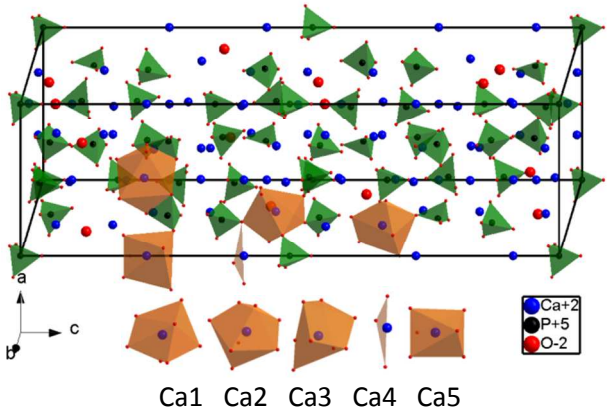

Fig. 4 Crystal structure of β-$Ca_3(PO_4)_2$ and different coordination environments for five kinds of Ca atoms.

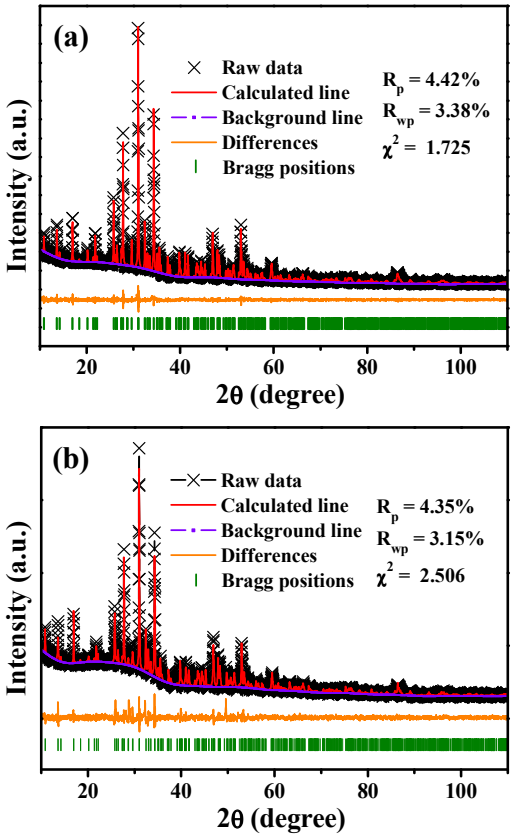

Fig. 5 Rietveld refinements of powder XRD profiles of representative β-CPO: 0.01Eu^{2+} (a) and β-CPO:0.01Eu^{2+}, 0.20Tb^{3+} (b) samples.

CPO:0.01Eu^{2+} and β-CPO:0.01Eu^{2+}, 0.20Tb^{3+} were conducted by GSAS program[40] in order to better understand the consistent degree of obtained XRD patterns with the structure. Fig. 5 presents the experimental values, calculated values, peak positions and difference of Rietveld refinement XRD patterns of β-CPO:0.01Eu^{2+} (Fig. 5a) and β-CPO:0.01Eu^{2+}, 0.20Tb^{3+} (Fig. 5b). The refined results indicate that all atom coordinates, fraction factors, as well as thermal vibration parameters were fitted well the reflection condition, R_p = 4.42%, R_{wp} = 3.38% and χ^2 = 1.725 for β-CPO:0.01Eu^{2+} and R_p = 4.35%, R_{wp} = 3.15% and χ^2 = 2.506, which demonstrate the little influence to crystal structure for the incorporations of Eu^{2+} and Tb^{3+}

Table 1 Crystallographic data and details in the data collection and refinement parameters for the β-CPO:0.01$Eu^{2+}$and β-CPO:0.01Eu^{2+}, 0.20Tb^{3+} phosphors.

Space group	*R3c*	*R3c*
Symmetry	rhombohedral	rhombohedral
a, Å	10.4494(1)	10.4457(1)
b, Å	10.4494(1)	10.4457(1)
c, Å	37.3887 (8)	37. 4012 (4)
V, Å^3	3535.49(12)	3534.22(5)
Z	21	21
2θ-interval, °	10-110	10-110
R_p	4.42	4.35
R_{wp}	3.38	3.15
χ^2	1.725	2.506

ions. In addition, the details on the data collection and refinement parameters are summarized in Table 1.

3.3 Photoluminescence properties

Fig. 6 shows the PL emission and excitation spectra of β-CPO:0.01Eu^{2+} sample. Upon 280 nm excitation, the emission spectrum presents an asymmetric broad band extending from 365 to 600 nm, which can be decomposed into five symmetric broad bands peaked at 390, 408, 421, 435, and 511 nm by Gaussian fitting based on five kinds of Ca sites for occupation by Eu^{2+} ions, respectively. According to the earlier discussion proposed by Van Uitert, the emission wavelength position of Eu^{2+} ion often strongly depends on its local environment, which can be estimated by following formula:[41]

$$E = Q\left[1-\left(\frac{V}{4}\right)^{\frac{1}{V}} 10^{-\frac{n\times Ea\times r}{80}}\right] \quad (1)$$

where E refers to the position of the d-band edge in energy for the rare-earth ion (cm^{-1}), Q is the position in energy for the lower d-band edge for the free ion (Q = 34000 cm^{-1} for Eu^{2+}), V corresponds to the valence of the "active" cation (V = 2 for Eu^{2+}), n is the number of anions in the immediate shell around the "active" cation, E_a refers to the electron affinity of the atoms that form anions (eV), which is variant when Eu^{2+} is introduced into different anion compounds with different coordination numbers while a constant for the same host, r is the radius of the host cation (Ca^{2+}) substituted by the "active" cation (Eu^{2+}). Considering the equation above, we can easily infer that the value of E is proportional to the quantity of r and n. Therefore, we can conclude that the bands centered at 390, 408, 421, 435, and 511 nm (25641, 24510, 23753, 22989 and 19569 cm^{-1} in inset of Fig. 6, respectively) correspond to Eu^{2+} occupying eight, eight, seven, six, and three-coordinated Ca^{2+} sites, respectively. However, the bands centered at 390 and 408 nm corresponding to which site (Ca2/Ca3) have not been identified. According to the proposal by Sun et al. and Jang et al., crystal field splitting (D_q) is usually estimated by the following expression:[42]

$$D_q = \frac{1}{6} Ze^2 \frac{r^4}{R^5} \quad (2)$$

where D_q refers to a measure of the energy level separation, Z corresponds to the anion charge, e is the electron charge, r is the radius of the d wave function, and R corresponds to the bond length. Reference 36 points out that the volume of Ca2-O8 polyhedron (26.08 Å^3) is bigger than that of Ca3-O8 (25.99 Å^3), which indicates that the average bond length of Ca2-O8 is

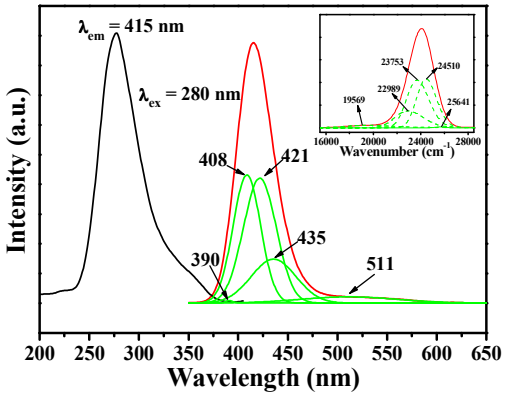

Fig. 6 PL excitation and emission spectra of β-CPO:0.01Eu^{2+} sample and the Gaussian fitting of the emission into five emissions. Inset is the corresponding fitting emissions plotted with wavenumber.

longer than that of Ca3-O8. Taking into the above equation, we can deduce the D_q of Ca3-O8 polyhedron is stronger than that of Ca2-O8, resulting in the longer emission when doped with Eu^{2+} ions. Therefore, the emission band centered at 390 nm is originated from Eu^{2+} occupying Ca2 sites, whereas the band around 408 nm belongs to Eu^{2+} occupying Ca3 sites. Monitored at 415 nm, the unresolved PL excitation spectrum comprises of a broad band ranging from 240 to 390 nm originated from Eu^{2+} 4f-5d allowed transition, which can be matched with UV LED chips.

The emission spectra of different concentration of Eu^{2+} single doped samples excited by 280 nm have been presented in Fig. 7. We can observe that the emission intensity increases with the increment of Eu^{2+} concentration until x = 0.01, and then it decreases with further concentration based on concentration quenching. Therefore, β-CPO: 0.01Eu^{2+} sample has the largest intensity in as-prepared samples. Thus we adopt the 0.01Eu^{2+} in the Eu^{2+}, Tb^{3+} co-doped β-CPO samples. Concentration quenching effect is generally originated from the energy transfer among Eu^{2+} ions in the host. In order to determine the energy transfer mechanism in β-CPO:xEu^{2+} samples, it is necessary to know the critical distance (R_c) between activators such as Eu^{2+} here. With the increasing of Eu^{2+} content, the distance between Eu^{2+} ions becomes shorter and shorter, thus the probability of energy migration increases. When the distance reaches small enough, the concentration quenching occurs and the energy migration is hindered. Therefore, the calculation of R_c has been pointed out by Blasse:[43,44]

$$R_c \approx 2\left[\frac{3V}{4\pi X_c N}\right]^{1/3} \quad (3)$$

where V corresponds to the volume of the unit cell, N is the number of host cations in the unit cell, and X_c refers to the critical concentration of dopant ions. For the β-CPO host, N = 21, V = 3520.91 Å^3, and X_c is 1% for Eu^{2+}; Accordingly, the critical distance (R_c) was estimated to be about 31.76 Å.

In general, three non-radiate energy transfer mechanisms include an exchange coupling, reabsorption of radiation, and via a multipolar interaction. The result obtained above indicates the little possibility of exchange interaction since the exchange interaction is predominant only for about 5 Å.[45] Since the reabsorption of radiation mechanism requires the widely overlapping of fluorescence and absorption spectra, it does not

intend to occur in this case. Therefore, the multipolar interaction contributes to the non-radiate energy transfer mechanism for this case. To investigate the energy-transfer behavior among Eu^{2+} ions for concentration quenching effect, we plot the linear fitting of log(x) versus log(I/x) for the β-CPO:xEu^{2+} phosphors beyond the quenching concentration in Fig. 8. According to the formula proposed by Dexter and Van Uitert, which can be expressed as follow:[46,47,48]

$$\frac{I}{x} = \left[1 + \beta\left(x\right)^{\theta/3}\right]^{-1} \quad (4)$$

where I represents the emission intensity, x refers to the activator ion concentration, and β is a constant for the given matrix under the identical excitation conditions. The type of energy transfer mechanism of electric multipolar interaction can be estimated by analyzing the constant θ from this formula. The value of θ = 6, 8, 10, corresponds to electric dipole-dipole, dipole-quadrupole or quadrupole-quadrupole interactions, respectively. Seen from the Fig. 8, the slope of fitting line is -θ/3 = -1.73, as a consequence, the θ is approximately as 6, indicating the dipole-dipole interactions dominates the energy transfer mechanism among Eu^{2+} in β-CPO:Eu^{2+} phosphors.

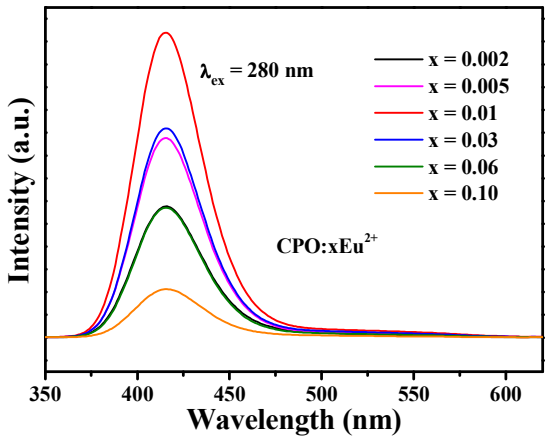

Fig. 7 Variation of emission spectra of β-CPO:xEu^{2+} with different concentration x for Eu^{2+} upon 280 nm UV radiation.

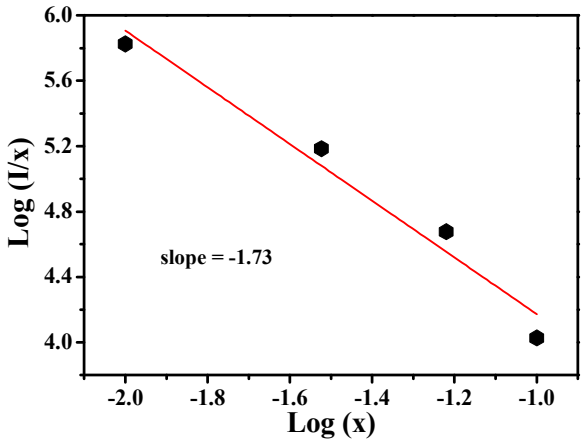

Fig. 8 Linear fitting of log(x) versus log(I/x) for the β-CPO:xEu^{2+} phosphors beyond the quenching concentration.

Tb^{3+}, a green activator frequently, has been investigated in detail in many hosts.[49-51] Additionally, it can be well introduced into this host as an effective activator. Here, we obtained a series of Tb^{3+} single doped β-CPO samples. Fig. 9a shows the PL excitation of β-CPO:0.20Tb^{3+} and emission spectra of β-CPO:yTb^{3+} with the Tb^{3+} concentration y = 0.001-0.30. Monitored at 547 nm, the excitation spectrum involves a band centered at 223 nm resulting from the 4f-5f allowed transition of Tb^{3+} ion and many lines at about 264, 287, 321, 341, 355, 380, 487 nm corresponding to its spin-forbidden transitions. Upon 223 nm excitation, the emission spectra present their characteristic emission lines resulting from $^5D_3$-^7F_J (J = 6,5,4,3,2) and $^5D_4$-^7F_J (J = 6,5,4,3) transitions, which cover the blue emission from the $^5D_3$ level and the green emission from the $^5D_4$ level, respectively. In the emission spectra for low doping concentrations (y < 0.01), the $^5D_3$-^7F_J transitions are dominant, and, the $^5D_4$-$^7F_5$ transition at 547 nm is dominant at higher doping concentrations (y > 0.01). Firstly, both transitions are enhanced with the increasing Tb^{3+} concentration. However, the emission intensity of former saturates at y = 0.01, which is different from the later at 0.20, which can be observed in Fig. 9b. It is well accepted that the energy gap between the $^5D_3$ and $^5D_4$ levels is close to that between $^7F_6$ and $^7F_0$ ones, which usually results in cross relaxation by the resonant energy-transfer process: $^5D_3$ (Tb^{3+}) + $^7F_6$ (Tb^{3+}) - $^5D_4$ (Tb^{3+}) + $^7F_0$ (Tb^{3+}).[52] Therefore, the cross relaxation arouses the quenching of the blue emissions of $^5D_3$ -^7F_J transitions, while the decrease of $^5D_4$-^7F_J transitions intensity is attributed to the concentration quenching effect.

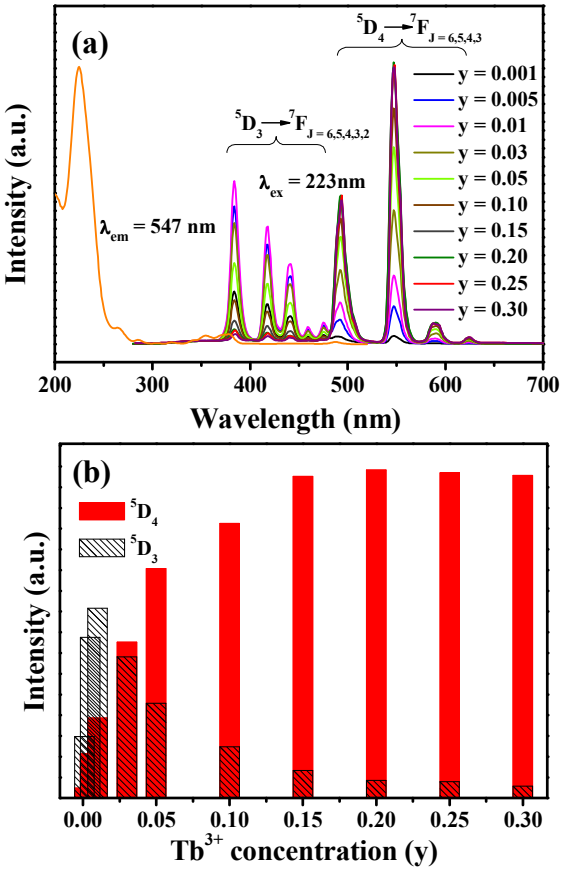

Fig. 9 (a) The PL excitation and emission spectra of β-CPO:yTb^{3+} phosphors. (b) The variation of emission intensity of $^5D_4$ and $^5D_3$ transitions as a function of Tb^{3+} concentration under 223 nm excitation.

3.4 Energy transfer mechanism

Fig. 10 illustrates the PL excitation and emission spectra of β-CPO:0.01Eu^{2+}, 0.30Tb^{3+} phosphor. Upon 320 nm excitation, the emission spectrum presents both Eu^{2+} emission band around 415 nm and Tb^{3+} emission lines of $^5D_4$-^7F_J. The Tb^{3+} emission intensity is much stronger than that of Eu^{2+}, which makes the sample present green color under a 365 nm UV lamp excitation. Monitored at 415 nm, the excitation spectrum displays a wide band which is identical with that in Eu^{2+} single doped β-CPO sample. The excitation spectrum detected at 547 nm shows both Eu^{2+} excitation band and Tb^{3+} characteristic excitation, which provides the possible existence of energy transfer from Eu^{2+} to Tb^{3+} ions in β-CPO:Eu^{2+}, Tb^{3+} phosphors. The variation of emission spectra and emission intensity of β-CPO:0.01Eu^{2+}, zTb^{3+} with different concentration z of Tb^{3+} ions are displayed in Fig. 11. All the Eu^{2+}, Tb^{3+} co-doped β-CPO samples have the emission bands of Eu^{2+} and Tb^{3+} ions excited at 320 nm in Fig. 11a. With increasing Tb^{3+} concentration z in β-CPO:0.01Eu^{2+}, zTb^{3+} phosphors, the emission spectra of Eu^{2+} section become weaker while stronger for Tb^{3+} area. Fig. 11b shows the dependence of emission intensity of Eu^{2+} and Tb^{3+} ions on the Tb^{3+} concentration z in β-CPO:0.01Eu^{2+}, zTb^{3+} samples, which illustrates the monotonous decent for Eu^{2+} emission and ascent for Tb^{3+} emission. Herein, we do not observe the concentration quenching effect in this case. The result gives the confirmation of energy transfer from Eu^{2+} to Tb^{3+} ions. Fig. 12 presents the decay curves (λ_{ex} = 320 nm, λ_{em} = 415 nm) of β-CPO: 0.01Eu^{2+}, zTb^{3+} (z = 0-0.40) samples with various Tb^{3+} concentration. The decay lifetimes can be approximately assessed using following equation:[53]

$$\tau = \int_0^\infty I(t)dt \qquad (5)$$

where τ refers to the calculated lifetime value, and $I(t)$ is the normalized intensity of emission curves. The lifetimes are evaluated to be 674, 636, 626, 576, 510 ns corresponding to z = 0, 0.10, 0.20, 0.30, 0.40. This monotonous decrease in lifetime with increasing Tb^{3+} concentration also certifies the existence of energy transfer from Eu^{2+} to Tb^{3+} ions. The energy transfer efficiency (η_T) from Eu^{2+} to Tb^{3+} ions in in β-CPO:0.01Eu^{2+}, zTb^{3+} samples can be approximately calculated using the formula as follow:[54,55]

$$\eta_T = 1 - \frac{I_S}{I_{S0}} \qquad (6)$$

where η_T refers to the energy transfer efficiency and I_{S0} and I_S are the luminescence intensity of Eu^{2+} ions in the absence and presence of Tb^{3+} ions, respectively. As depicted in Fig. 13, the energy transfer efficiency ascends monotonously with continuously increasing Tb^{3+} concentration (η_T = 21.5-92.2% corresponding to z = 0.05-0.40) while the increasing rate decreases because the stationary Eu^{2+} concentration restricts the energy transfer from Eu^{2+} ions to Tb^{3+} ions. Fig. 14 shows the CIE chromaticity coordination for β-CPO:0.01Eu^{2+}, zTb^{3+} phosphors (1-8) under 280 nm excitation, and the luminescence photographs of corresponding phosphors excited under a 365 nm UV lamp on the right of picture. The CIE chromaticity coordination shifts from (0.169, 0.031) to (0.281, 0.509) corresponding to z = 0 and 0.40 in β-CPO:0.01Eu^{2+}, zTb^{3+} phosphors, respectively, which is in accordance with the variation of luminescence photographs under a 365 nm UV lamp excitation. The detailed value of CIE chromaticity coordinates and quantum efficiencies for corresponding samples are listed in Table 2. We observe the maximum quantum efficiency can reach 90% for β-CPO:0.01Eu^{2+}, 0.15Tb^{3+} with the absorption efficiency 47%, which is considered to be anticipated and potential as a candidate phosphor for wLED fabrication, and it may be optimized via

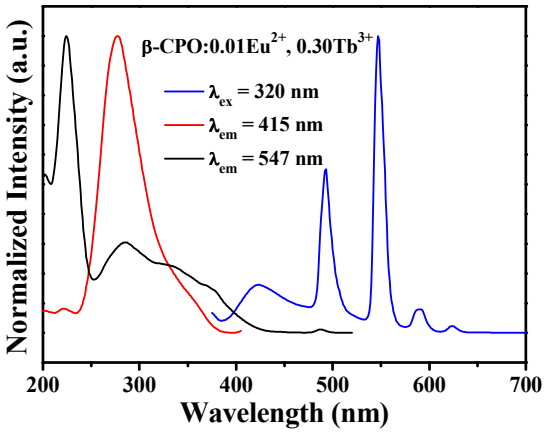

Fig. 10 PL excitation spectra monitored at 415 and 547 nm and emission spectrum excited at 320 nm for β-CPO:0.01Eu^{2+}, 0.30Tb^{3+}.

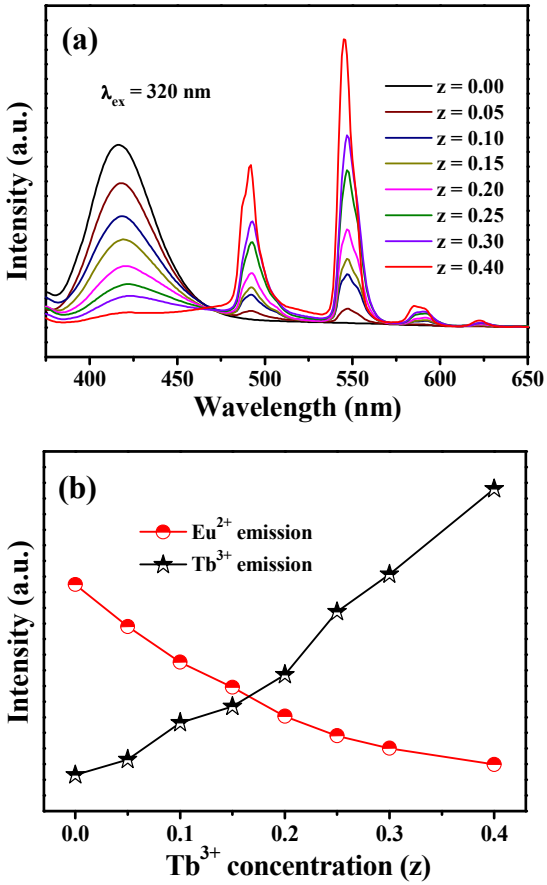

Fig. 11 (a) Variation of emission spectra of β-CPO:0.01Eu^{2+}, zTb^{3+} with different concentration z of Tb^{3+}. (b) Dependence of emission intensity of Eu^{2+} and Tb^{3+} ions on the Tb^{3+} concentration z in β-CPO:0.01Eu^{2+}, zTb^{3+} samples.

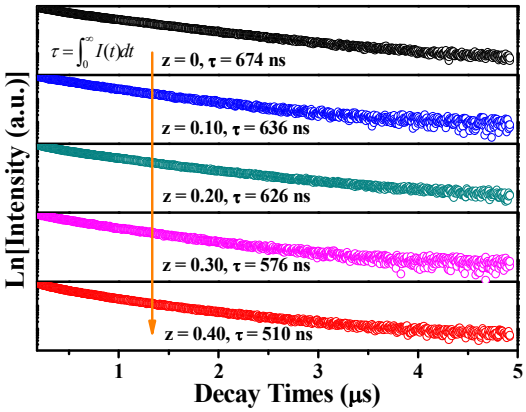

Fig. 12 Dependence of decay curves and calculated decay lifetimes on Tb^{3+} concentration z in β-CPO:0.01Eu^{2+}, zTb^{3+} phosphors (λ_{ex} = 320 nm, λ_{em} = 415 nm).

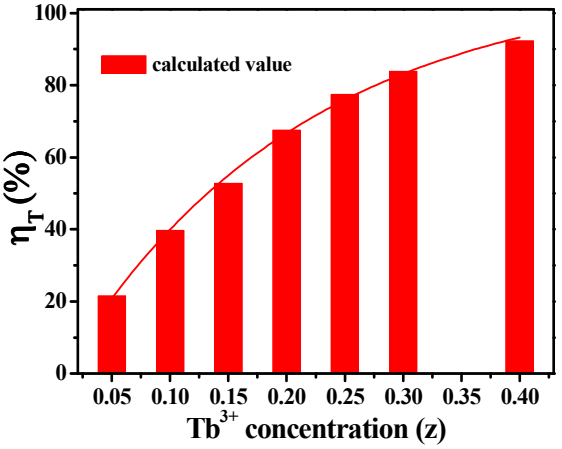

Fig. 13 Variation of calculated energy transfer efficiency (η_T) value from Eu^{2+} to Tb^{3+} ions as a function of Tb^{3+} concentration z in β-CPO:0.01Eu^{2+}, zTb^{3+} phosphors.

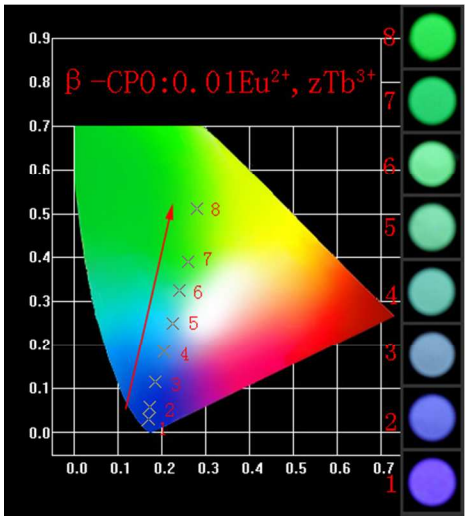

Fig. 14 CIE chromaticity coordination for β-CPO:0.01Eu^{2+}, zTb^{3+} phosphors (1-8) under 280 nm excitation, and the luminescence photographs of corresponding phosphors excited under a 365 nm UV lamp are showed on the right of picture.

Table 2 The variation of CIE chromaticity coordinates (x, y) and quantum yields (QYs) for β-CPO:0.01Eu^{2+}, zTb^{3+} phosphors excited at 280 nm UV radiation.

Sample No.	Tb^{3+} concentration (z)	CIE coordinates (x, y)	QY (%)	Absorption (%)
1	0	(0.169, 0.031)	84	37
2	0.05	(0.173, 0.057)	81	33
3	0.10	(0.186, 0.115)	82	44
4	0.15	(0.205, 0.185)	90	47
5	0.20	(0.225, 0.250)	59	30
6	0.25	(0.240, 0.325)	60	27
7	0.30	(0.259, 0.389)	56	29
8	0.40	(0.281, 0.509)	45	22

the better synthesis processing and chemical composition.

As described in Eu^{2+} singly doped β-CPO part above, for this host, the R_c is calculated to be 12.11 Å via using the equation 3, where the different value of X_c is defined as the critical concentration of dopant ions (total concentration of Eu^{2+} and Tb^{3+}, approximately 0.18), that is, at which the luminescence intensity of Eu^{2+} is half of that in the sample without Tb^{3+}. Since the value of R_c is much longer than 5 Å, which implies the exchange interaction would not be responsible for the energy transfer mechanism from Eu^{2+} to Tb^{3+} ions. As a result, we can infer that the electric multipolar interactions will take place for energy transfer between Eu^{2+} and Tb^{3+}. On account of Dexter's energy transfer formula of multipolar interaction and Reisfeld's approximation, the following relationship can be attained:[56]

$$\frac{\eta_{S0}}{\eta_S} \propto C^{\alpha/3} \quad (7)$$

where η_{S0} and η_S represent the luminescence quantum efficiencies of the Eu^{2+} ions with the absence and presence of the Tb^{3+} ions, respectively. C is the total concentration of the Eu^{2+} and Tb^{3+} ions. The value for α = 6, 8, and 10 corresponds to dipole-dipole, dipole-quadrupole, and quadrupole-quadrupole interactions, respectively. However, the value of η_{S0}/η_S is hard to be obtained and therefore it can be approximately calculated instead by the I_{S0}/I_S, where I_{S0} and I_S stand for the luminescence intensity of the Eu^{2+} ions without and with the Mn^{2+} ions, respectively, the following relation can be obtained:[57]

$$\frac{I_{S0}}{I_S} \propto C^{\alpha/3} \quad (8)$$

The relationship between I_{S0}/I_S and $C^{\alpha/3}$ based on the above equation are illustrated in Fig. 15. Only R = 8 can the linear relation be observed, indicating that the energy transfer from Eu^{2+} to Tb^{3+} ions takes place through the dipole-quadrupole interactions mechanism.

The energy transfer critical distance (R_c) between Eu^{2+} and Tb^{3+} ions also can be obtained through spectral overlap method, which can be expressed by the following equation:[58]

$$R_c^8 = 3.024 \times 10^{12} \lambda_S^2 f_q \int f_S(E) f_A(E) / E^4 dE \quad (9)$$

where f_q is the oscillator strength of Tb^{3+} dipole and quadrupole electrical absorption transitions, it is a pity that the oscillator strength of the Tb^{3+} quadrupole transition (f_q) has not been obtained up to now. However, it was suggested by Verstegen et al. that the ratio f_q/f_d is about 10^{-3}-10^{-2},[59] where $f_d = 10^{-6}$ is the

oscillator strengths of the electric dipole transitions. λ_S = 4150 Å is the wavelength of strongest intensity of Eu^{2+}; E is the energy involved in the transfer (in eV); $\int f_S(E) f_A(E)/E^4 dE$ represents the spectral overlap between the normalized shapes of the Eu^{2+} emission $f_S(E)$ and the Tb^{3+} excitation $f_S(E)$, and in our case it is calculated to be about 0.00177 eV^{-5}. Accordingly, the R_c value is calculated to be 9.9-13.2 Å, which is in accordance with that obtained above by concentration method. This can further certify the energy transfer mechanism from Eu^{2+} to Tb^{3+} ions in this host is to be electric dipole-quadrupole interactions.

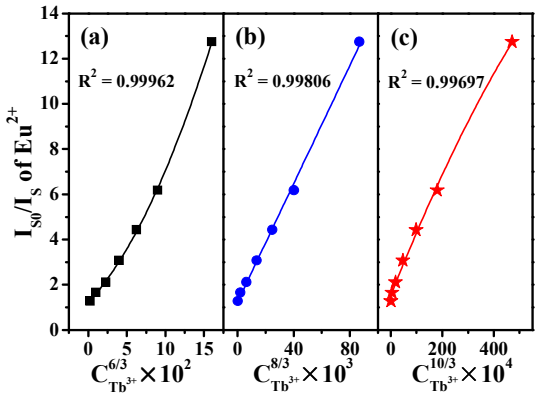

Fig. 15 Dependence of I_{S0}/I_S of Tb^{3+} on $C^{6/3}$ (a), $C^{8/3}$ (b), and $C^{10/3}$ (c).

3.5 Thermal quenching properties

Generally, the thermal stability is a crucial technology parameter for a phosphor that should be indispensable to be taken into account when applied in solid-state lighting, especially phosphor-conversion w-LEDs systems, owing to its influence on the light output and CRI. Accordingly, temperature-dependent emission spectra of as-prepared β-CPO:0.01Eu^{2+}, 0.30Tb^{3+} excited at 330 nm have been presented in Fig. 16a, which shows the continuous decrease of emission intensity with increasing temperature from 25 to 200℃. The integrated emission intensity of β-CPO:0.01Eu^{2+}, 0.30Tb^{3+} decreased to 45.7% (150℃) of the original value (25℃). This drop of emission intensity is attributed to the thermal quenching of emission intensity via phonon interaction, in which the excited luminescence center is thermally activated through the crossing point between the ground and the excited states.[60] To better understand the relationship between the PL and the temperature and calculate the activation energy from the thermal quenching, the Arrhenius equation was proposed below:[61]

$$I_T = \frac{I_0}{1 + c\exp\left(\frac{E_a}{-kT}\right)} \quad (10)$$

Herein, I_0 and I represent the emission intensity at room temperature and different operated temperatures, respectively, c is a constant for a certain host, E_a refers to activation energy of thermal quenching (which is the energy required to raise the electron from the relaxed excited level into the host lattice conduction band), and k is the Boltzmann constant (8.626×10^{-5} eV). According to the equation, the activation energy E_a can be calculated by plotting ln[(I_0/I)-1] against 1/kT in Fig. 16b,

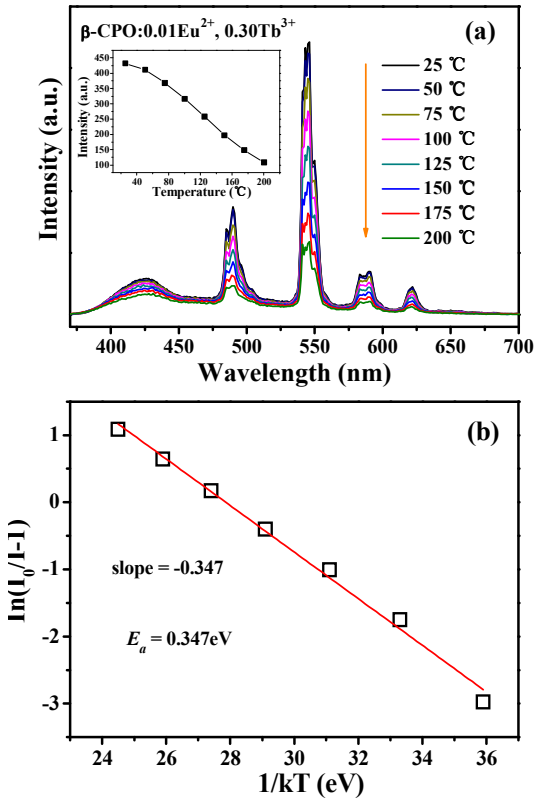

Fig. 16 (a) Temperature-dependent PL spectra of β-CPO:0.01Eu^{2+}, 0.30Tb^{3+} . The inset shows the relationship of relative intensity and temperature. (b) The ln[(I_0/I)-1] vs. 1/kT activation energy graph for thermal quenching of β-CPO:0.01Eu^{2+}, 0.30Tb^{3+} .

where a straight slope equals -E_a. Therefore, the E_a was calculated to be 0.347 eV from the slope of the fitting straight line.

4. Conclusions

In summary, a series of Eu^{2+} and Tb^{3+} singly and co-doped β-CPO phosphors have been prepared via the high-temperature solid-state reaction route. In β-CPO:0.01Eu^{2+}, the sample presents a broad emission band centered at 415 nm which can be resolved into five symmetrical bands peaking at 390, 408, 421, 435 and 511 nm attributed to Eu^{2+} occupying five kinds of Ca^{2+} sites under UV excitation. The Tb^{3+} singly doped β-CPO samples display their characteristic emission lines based on 4f-4f transitions of Tb^{3+}. When Eu^{2+} and Tb^{3+} are co-doped into β-CPO, the samples show tunable emission color from blue-purple to green attributed to the energy transfer from Eu^{2+} to Tb^{3+} ions under UV excitation, which can be deduced from the similar excitation spectra in β-CPO:Eu^{2+}, Tb^{3+} monitored at Eu^{2+} and Tb^{3+} emission band, and subsequently demonstrated from the variations of emission spectra and decay lifetimes. The energy transfer mechanism is illustrated to be dipole-quadrupole interactions, which is validated via the agreement of the R_c values calculated by the concentration quenching (12.11 Å) and spectrum overlap methods (9.9-13.2 Å). The maximum quantum efficiency is 90% for β-$Ca_3(PO_4)_2$:0.01Eu^{2+}, 0.15Tb^{3+} sample under 280 nm excitation. The investigation on the temperature-dependent PL indicates that the activation energy is 0.347 eV for β-

$Ca_3(PO_4)_2$:0.01Eu^{2+}, 0.30Tb^{3+} phosphor. It suggests the potential application of β-$Ca_3(PO_4)_2$:Eu^{2+}, Tb^{3+} in UV-pumped wLEDs.

Acknowledgments

This project is financially supported by the National Natural Science Foundation of China (91433110, 51172227, and 51472234), National Basic Research Program of China (2014CB643803), and Joint Funds of the National Natural Science Foundation of China (U13012042).

References

1 Y. Q. Li, A. C. A. Delsing, G. D. With and H. T. Hintzen, *Chem. Mater*., 2005, **17**, 3242.
2 K. Hanaoka, K. Kikuchi, T. Terai, T. Komatsu and T. Nagano, *Chemistry*, 2008, **14**(3), 987.
3 C. Liang, F. Li, C. Liu, J. Lu and X. Wang, *Dyes and Pigments*, 2008, **76**, 477.
4 K. Huang, W. Chen, C. Chu, S. Hu, H. Sheu, B. Cheng, J. Chen and R. Liu, *Chem. Mater*., 2012, **24**, 2220.
5 G. Lee, J. Y. Han, W. B. Im, S. H. Cheong and D. Y. Jeon, *Inorg. Chem*., 2012, **51**, 10688.
6 Y. H. Liu, J. H. Hao, W. D. Zhuang and Y. S. Hu, *J. Phys. D: Appl. Phys*., 2009, **42**, 245102.
7 Z. Ci, Q. Sun; S. Qin, M. Sun, X. Jiang, X. Zhang and Y. Wang, *Phys. Chem. Chem. Phys*., 2014, **16**(23), 11597.
8 Z. Xia and R. Liu, *J. Phys. Chem. C*, 2012, **116**, 15604.
9 S. K.K. Shaat, H. C. Swart and O. M. Ntwaeaborwa, *J. Alloys Compds*., 2014, **587**, 600.
10 R. Li, L. Li, W. Zi, J. Zhang, L. Liu, L. Zou and S. Gan, *New J. Chem*., 2014, DOI: 10.1039/C4NJ01136H.
11 G. Li, S. Lan, L. Li, M. Li, W. Bao, H. Zou, X. Xu and S. Gan, *J. Alloys Compd*., 2012, **513**, 145.
12 X. Zhou, X. Yang, T. Xiao, K. Zhou, Chen T., H. Yan and Z. Wang, *J. Rare Earth*, 2013, **31**, 655.
13 N. Guo, Y. Song, H. You, G. Jia, M. Yang, K. Liu, Y. Zheng, Y. Huang and H. Zhang, *Eur. J. Inorg. Chem*., 2010, **29**, 4636.
14 Y. Zhang, D. Geng, M. Shang, Y. Wu, X. Li, H. Lian, Z. Cheng and J. Lin, *Eur. J. Inorg. Chem*., 2013, **25**, 4389.
15 W. Lu, Z. Hao, X. Zhang, Y. Luo, X. Wang and J. Zhang, *Inorg. Chem*., 2011, **50**, 7846.
16 Y. Wen, Y. Wang, F. Zhang and B. Liu, *Mater. Chem. Phys*., 2011, **129**, 1171.
17 D. Wen and J. Shi, *Dalton Trans*., 2013, **42**, 16621.
18 C. Huang and T. Chen, *J. Phys. Chem. C*, 2011, **115**, 2349.
19 Y. Shi, G. Zhu, M. Mikami, Y. Shimomura and Y. Wang, *Mater. Res. Bull*., 2013, **48**, 114.
20 K. G. Tshabalala, S.-H. Cho, J.-K. Park, Shreyas S. Pitale, I. M. Nagpure, R. E. Kroon, H. C. Swart and O. M. Ntwaeaborwa, *J. Alloys Compd*., 2011, **509**, 10115.
21 D. Hou, C. Liu, X. Ding, X. Kuang, H. Liang, S. Sun, Y. Huang and Y. Tao, *J. Mater. Chem. C*, 2013, **1**, 493.
22 Y. Chiu, C. Huang, T. Lee, W. Liu, Y. Yeh, S. Jang and R. Liu, *Opt. Exp*., 2012, **19**, A331.
23 C. Huang, Y. Chiu, Y. Yeh and T. Chen, *Mater. Express*, 2012, **2**, 303.
24 W. B. Park, S. P. Singh, C. Yoon and K.-S. Sohn, *J. Mater. Chem*., 2012, **22**, 14068.
25 G. Zhu, S. Xin, Y. Wen, Q. Wang, M. Que and Y. Wang, *RSC Adv*., 2013, **3**, 9311.
26 W. Lu, Y. Jia, W. Lv, Q. Zhao and, H. You, *RSC Adv.*, 2013, **3**, 20619.
27 C. Huang and T. Chen, *Opt. Exp*., 2010, **18**, 5089.
28 N. Guo, H. You, Y. Song, M. Yang, K. Liu, Y. Zheng, Y. Huang and H. Zhang, *J. Mater. Chem*., 2010, **20**, 9061.
29 N. Guo, Y. Huang, H. You, M. Yang, Y. Song, K. Liu and Y. Zheng, *Inorg. Chem*., 2010, **49**, 10907.
30 C. Zhao, X. Yin, Y. Wang, F. Huang and Y. Hang, *J. Lumin*., 2012, **132**, 617.
31 C. Huang, P. Wu, J. Lee and T. Chen, *J. Mater. Chem*., 2011, **21**, 10489.
32 E. Song, W. Zhao, G. Zhou, X. Dou, C. Yi and M. Zhou, *J. Rare Earths*, 2011, **29**, 440.
33 D. Wei, Y. Huang, L. Shi, X. Qiao and H. J. Seo, *J. Electrochem. Soc*., 2009, **156**, H885.
34 D. Wen, Z. Dong, J. Shi, M. Gong and M. Wu, *ECS J. Solid State Sci. Technol*., 2013, **2**(9), R178.
35 F. Du, R. Zhu, Y. Huang, Y. Tao and H. J. Seo, *Dalton Trans*., 2011, **40**, 11433.
36 F. Du, Y. Nakai, T. Tsuboi, Y. Huang and H. J. Seo, *J. Mater. Chem*., 2011, **21**, 4669.
37 Y. Huang, C. Jiang, Y. Cao, L. Shi and H. J. Seo, *Mater. Res. Bull*., 2009, **44**, 793.
38 G. R. Dillip and B. D. P. Raju, *J. Alloys Compd*., 2012, **540**, 67.
39 M. Yashima, A. Sakai, T. Kamiyama and A. Hoshikawa, *J. Solid State Chem*., 2003, **175**, 272.
40 C. Larson, R. B. Von Dreele, Generalized Structure Analysis System (GSAS), Los Alamos National Laboratory Report LAUR 86-748, Los Alamos National Laboratory, Los Alamos, NM, 1994.
41 Z. Xia, J. Zhou and Z. Mao, *J. Mater. Chem. C*, 2013, **1**, 5917.
42 P. D. Rack and P. H. Holloway, *Mater. Sci. Eng. R*, 1998, 21, 171.
43 G. Blasse, *Philips Res. Rep*., 1969, **24**, 131.
44 N. Zhang, C. Guo, J. Zheng, X. Su and J. Zhao, *J. Mater. Chem. C*, 2014, **2**, 3988.
45 D. L. Dexter, *J. Chem. Phys*., 1953, **21**, 836.
46 L. G. Van Uitert, *J. Lumin*., 1971, **4**, 1.
47 G. Blasse, *Phys. Lett*., 1968, **28**, 444.
48 X. Zhao, L. Fan, T. Yu, Z. Li and Z. Zou, *Opt. Exp*., 2013, 21, 31660.
49 S. Cui, Y. Zhu, W. Xu, P. Zhou, L. Xia, X. Chen, H. Song and W. Han, *Dalton Trans*., 2014, **43**, 13293.
50 S. K.K. Shaat, H. C. Swart and O. M. Ntwaeaborwa, *J. Alloys Compd*., 2014, **587**, 600.
51 M. Zhang, Y. Liang, W. Huang, Z. Xia, D. Yu b, Y. Lan, G. Li and W. Zhou, *Mater. Res. Bull*., 2014, **57**, 231.
52 K.-S. Sohn, Y. Y. Choi, H. D. Park and Y. G. Choi, *J. Electrochem. Soc*., 2000, **147**, 2375.
53 K. Li, D. Geng, M. Shang, Y. Zhang, H. Lian and J. Lin, *J. Phys. Chem. C*, 2014, **118**, 11026.
54 K. H. Lee, S. Choi, H. Jung and W. B. Im, *Acta Mater*., 2012, **60**, 5783.
55 W. Tang, T. Fu, K. Deng and M. Wu, *Ceram. Inter*., 2013, **39**, 6363.
56 D. L. Dexter, *J. Chem. Phys*., 1953, **21**, 836.
57 D.L. Dexter and J. H. Schulman, *J. Chem. Phys*., 1954, **22**, 1063.
58 N. Guo, Y. Zheng, Y. Jia, H. Qiao and H. You, *J. Phys. Chem. C*, 2012, **116**, 1329.
59 J. M. P. J. Verstegen, J. L. Sommerdijk and J. G. Verriet, *J. Lumin*., 1973, **6**, 425.
60 J. S. Kim, Y. H. Park, S. M. Kim, J. C. Choi and H. L. Park, *Solid State Commun*., 2005, **133**, 445.

61 S. Bhushan and M. V. Chukichev, *J. Mater. Sci. Lett.*, 1988, **7**, 319.

Graphic Abstract

A series of Eu^{2+} and Tb^{3+} singly doped and co-doped β-$Ca_3(PO_4)_2$ phosphors have been synthesized via the high-temperature solid-state reaction method. The emission color can be tuned from blue to green through adjusting Eu^{2+}/Tb^{3+} concentration ratio, which shows the potential application in UV-pumped white-light-emitting diodes.